

Article

Methodology for the Prediction of Water Gushing in Tunnels in Igneous Fracture Tectonic Zones: A Case Study of a Tunnel in Guangdong Province, China

Weifeng Zhang¹, Xuemin Zhou¹, Baoyong Wang², Xiaoyong Cheng³ and Wei Wei^{1,*}

¹ College of Water Conservancy and Civil Engineering, South China Agricultural University, Guangzhou 510642, China

² College of Water Resources Science and Engineering, University of Zhengzhou, Zhengzhou 450001, China

³ Guangdong Communication Planning & Design Institute Group Co., Ltd., Guangzhou 510507, China

* Correspondence: w_f_zh@126.com; Tel.: +86-13711030601

Abstract: The disaster of water gushing is very liable to occur when tunnels are built in the water-rich fracture structures in igneous rock areas. Different sources of water gushing result in different sizes of disaster. The safety of human life and property are in danger. For the prediction of water gushing in tunnels, the fuzzy clustering method was used to determine the source of the water gushing in this paper. The problem of subjectivity in traditional identification methods was solved by this method. On the basis of the fuzzy clustering method, dynamically changing parameters of the effective radius of the water gushing were introduced and regressed with the dynamic monitoring data and the hydrogeological survey results in an improved method for predicting water gushing. Then, an improved method for predicting water gushing, considering the source, was proposed. A deep underground, extra-long tunnel under construction in the igneous region of southern China was used to verify the soundness of this improved method. Research results showed that the water gushing into the tunnel had a low correlation with surface water with a similarity index of $\lambda_{min} = 0.3967$ in the results of the second test. The water came mainly from within the rock mass. The effective radius were jointly determined by the average thickness of the rock aquifer and water gushing time, together with a positive correlation. The period of water gushing was divided into three stages. The predictions had a good accuracy rate with an error of 10% or less. These results could provide a reference and theoretical support for site construction.

Keywords: deeply buried mountain tunnel; fault; fuzzy clustering method; effective radius of water gushing; dynamic prediction of water gushing



Citation: Zhang, W.; Zhou, X.; Wang, B.; Cheng, X.; Wei, W. Methodology for the Prediction of Water Gushing in Tunnels in Igneous Fracture Tectonic Zones: A Case Study of a Tunnel in Guangdong Province, China. *Appl. Sci.* **2022**, *12*, 10438. <https://doi.org/10.3390/app122010438>

Academic Editor: Daniel Dias

Received: 11 August 2022

Accepted: 14 October 2022

Published: 16 October 2022

Publisher's Note: MDPI stays neutral with regard to jurisdictional claims in published maps and institutional affiliations.



Copyright: © 2022 by the authors. Licensee MDPI, Basel, Switzerland. This article is an open access article distributed under the terms and conditions of the Creative Commons Attribution (CC BY) license (<https://creativecommons.org/licenses/by/4.0/>).

1. Introduction

Mountain tunnels often have to cross fracture zones and karst areas, where undesirable geological bodies are hidden and construction conditions in mountainous areas are far more complex than those in urban areas [1]. During construction, the site is frequently exposed to hazards, such as water gushing [2,3]. In particular, when deeply buried tunnels cross water-rich fracture zones, large amounts of high-pressure groundwater will rush into the tunnel through the fracture zones in a short period of time. The lives and property of workers will be at risk [4], and the local ecology will be negatively affected [5–7].

Aiming at the problem of water gushing caused by water-rich fracture tectonic zones, scholars have carried out various types of approaches to model predictions for tunnels [1,8–10]. Zhang et al. [11] believed that the dynamic characteristics of groundwater can be replicated by in-situ monitoring and numerical simulation to predict tunnel gushing. Sun et al. [12] analysed the formation and evolution of water gushing channels on deeply buried faults using Comsol software, which has positive implications for the prediction of

water gushing on faults. Li et al. [13] applied numerical simulations to show the characteristics of water gushing in the excavation phase based on electromagnetic geophysical prospecting. Based on the Darcy–Brinkman flow equation, Wu et al. [14] explores the behaviour of groundwater flow in faults to obtain the evolution of pore pressure and flow velocity at different locations, which provides a reference for the prediction of water gushing in fractured tectonic zones. In addition, it is important to determine the source of water in the process of predicting the amount of water gushing [15,16]. This supports engineers in predicting the size of the water gushing. The fuzzy clustering method and the hydro-geochemistry method could also be used to identify the source of water gushing, even though they were more commonly employed for groundwater quality monitoring, such as the work performed in reference [17]. Wang et al. [18], Chen et al. [19], and others analysed the data from the above method and identified the source of water gushing in subterranean space. Kang et al. [20] applied a fuzzy clustering method and the hydro-geochemistry method to identify the source of water gushing and provide data support for the prediction of water gushing.

In general, various new methods for the prediction of water gushing have progressed considerably in terms of depth of research, but not enough attention has been paid to the identification of sources of water gushing. In practice, the fuzzy clustering method and the hydro-geochemistry method are rarely used in combination to identify the source of water gushing. The results derived from the hydro-geochemistry method rely more on the experience of the engineers to analyse and judge, and do not apply the fuzzy clustering method scientifically. Meanwhile, less research has been carried out on areas of fractured tectonic zones with developing groundwater in igneous rocks, which are hard and stable [21,22] and, as such, are often considered ideal areas for underground construction. At this stage, the applicability of the new methods is limited by the limitations and complexity of geological investigation techniques [23,24]. Indeed, there are fewer theoretical studies on bedrock fracture water flow in deep alpine layers, fewer hydrogeological tests conducted in the field [25], and the high cost of trials is an obstacle to their application. In addition, engineers prefer to apply traditional methods of prediction, in which the effective radius of the water gushing is regarded as a fixed value by traditional methods and the flow field in the tunnel site area is also simplified in general terms. Admittedly, they are intuitive and simple, but large deviations are often found. Similarly, the identification of the source of water gushing is mainly dependent on the analysis of geological survey data by experienced engineering personnel in the traditional approach. The process is highly subjective and poorly suited to complex processes [26]. Survey data from construction sites should be analysed using more scientific and effective methods.

Hence, the method used in this study improves on them for the prediction of water gushing in the tunnel to make up for their shortcomings. Ultimately, there is a more accurate set of methods for water gushing in deep underground, extra-long tunnels in igneous areas. In this study, the improved method could meet the needs of the project. The analysis of the sources had been given more emphasis, as well as the complex aquifer structure, which could be simplified to some extent. A deep underground, extra-long tunnel under construction in an igneous region of southern China was used as the research object. With the help of the hydrogeological survey results of the water-rich fracture zone in the pre-construction period and the monitoring data of water gushing in the excavation period, the fuzzy clustering method was used to determine the source of water gushing. The water gushing caused a strong drop in groundwater level in the tunnel site area. By analysing the characteristics of water gushing within a rainfall cycle, the pattern of change in the effective radius of the groundwater fall funnel could be investigated. Based on curve-fitting means, a predictive model can be constructed for the amount of water that can be predicted in a tunnel project across a fracture zone. Some of the references are provided by the above model for subsequent works of the same type.

2. Fuzzy Clustering Method

A fuzzy matrix is constructed by the fuzzy clustering method based on the structure and changing characteristics of the data, and they are classified and divided according to the transfer closure method. A finite theoretical domain U with n samples and a fuzzy assessment set V with m assessment values are assumed. Here, U and V can be expressed by Equations (1) and (2) [27,28], as follows:

$$U = \{u_1, u_2, \dots, u_n\}, \tag{1}$$

$$V = \{v_1, v_2, \dots, v_m\}. \tag{2}$$

The original data matrix Z is built up according to U and V . Here, Z is defined as follows:

$$Z = \begin{pmatrix} z_{11} & \cdots & z_{1m} \\ \vdots & \ddots & \vdots \\ z_{n1} & \cdots & z_{nm} \end{pmatrix}, \tag{3}$$

where z_{nm} is the value of the m -th assessment indicator for the n -th sample. Based on the raw data obtained, the three steps of the fuzzy clustering method are executed as follows:

Step 1. Standardisation of the original data matrix Z . The original data matrix Z was standardised by the following Equation (4):

$$z'_{ik} = \frac{z_{ik} - \frac{1}{n} \sum_{i=1}^n z_{ik}}{\sqrt{\frac{1}{n} \sum_{i=1}^n (z_{ik} - \frac{1}{n} \sum_{i=1}^n z_{ik})^2}}, \tag{4}$$

and the following Equation (5) [29,30]:

$$z''_{ik} = \frac{z'_{ik} - \min z'_{ik}}{\max z'_{ik} - \min z'_{ik}}. \tag{5}$$

The standardisation matrix Z'' was obtained, which could be expressed as follows:

$$Z'' = \begin{pmatrix} z''_{11} & \cdots & z''_{1n} \\ \vdots & \ddots & \vdots \\ z''_{m1} & \cdots & z''_{mn} \end{pmatrix}; (i = 1, 2, \dots, n; k = 1, 2, \dots, m). \tag{6}$$

Step 2. Construction of fuzzy similarity matrix. The fuzzy similarity matrix $C = [c_{ij}]_{nm}$ was obtained from the above Z'' using the following Equation (7):

$$\begin{cases} c_{ij} = 1 - \sum_{k=1}^m |z''_{ik} - z''_{jk}| \\ c_{ij} = c_{ji} \\ c_{ii} = 1 \end{cases}. \tag{7}$$

According to the squared self-synthesis method, the matrix C was squared by the following:

$$\begin{cases} C^\sigma \circ C^\sigma = C^{2\sigma} (\sigma = 1, 2, \dots) \\ c^2_{ij} = \bigvee_{k=1}^m (c_{ik} \wedge c_{jk}) \end{cases}. \tag{8}$$

to obtain the fuzzy equivalence matrix $C^* = [c^*_{ij}]_{nm}$, where $\bigvee_{k=1}^m$ represented the selection of the item with the largest value among the m numbers; \wedge represented the selection of the one with the smallest value among the m numbers; σ was a natural number. When

$C^{2k} = C^{2(k+1)}$, C^{2k} was already transmissible, at which point $C^* = t(C) = C^{2k}$ was satisfied. Then, the fuzzy equivalence matrix C was identified.

Step 3. Cluster analysis. There existed a similarity index λ as a threshold for sample similarity classification, by which the samples could be classified into several classes.

The classification criteria in this paper were simplified based on the criteria proposed by Yang et al. [31]. When $\lambda \in [0, 1]$, the value of λ would directly affect the accuracy of the classification. If $\lambda > 0.6$, the samples were considered correlated. Furthermore, if $0.3 \ll \lambda \ll 0.6$, they were considered to be weakly correlated with each other. Then, if $\lambda < 0.3$, they were considered uncorrelated.

3. Prediction of Water Gushing in Tunnels

When tunnels are built through the water-rich fracture structures in igneous rock areas, the amount of water gushing in tunnels will occur in each day of excavation. If the effects of the unexcavated section of the tunnel far from the tunnel face are always taken into account in the calculations, that will cause large calculation errors in the prediction of water gushing. At this point, the combined effect of the areas of water-rich fault fracture zones and construction factors should be considered. The constructed tunnel sections and those, where the aquifer is disturbed, are segmented for the prediction of water gushing [7]. The tunnel is divided into N sections, and the daily excavation gushing can be set as Q . The calculation formula is given in Equation (9), as follows:

$$Q = \sum_{n=1}^N Q_n. \tag{9}$$

The water gushing in the tunnel is generally derived into two major parts. One is from water released from bedrock fracture water, and the other is from the infiltration of rainfall. They are expressed with reference to Equation (10), as follows:

$$Q = W_{n(1)} + W_{n(2)}, \tag{10}$$

where Q_n is the total water gushing in the n -th section of the tunnel, m^3/d ; N is the total number of sections of tunnel that have been constructed in a given period and in which the aquifer has been disturbed; $W_{n(1)}$ is the amount of water released from bedrock fractures, m^3/d ; $W_{n(2)}$ is the amount of rainfall infiltration, m^3/d . An example of a tunnel section division is shown in Figure 1.

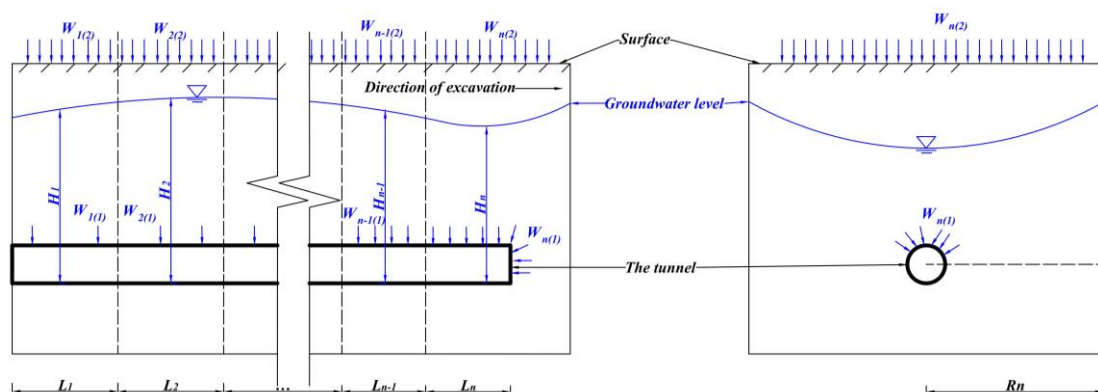


Figure 1. Example diagram of a tunnel section.

When all the water is released from the bedrock fractures, $W_{n(2)} = 0$. Conversely, when the water is infiltrated by rainfall, $W_{n(1)} = 0$. If both of these are deemed to exist, $W_{n(1)}$ and $W_{n(2)}$ continue to be determined in the following manner.

With a well-developed fracture network and good permeability, the aquifer in the tunnel site area is large in scale, and the storage capacity of water from bedrock fracture

is huge. The water released from bedrock fracture can be calculated by the groundwater drainage method. It can be expressed as $W_{n(1)}$, which is calculated by the following Equation (11) [32,33]:

$$W_{n(1)} = \frac{\mu L_n H_n R_n}{T}, \quad (11)$$

where μ is the specific yield of rock; L_n is the length of the n -th segment, m; H_n is the average thickness of the aquifer above the n -th tunnel section, m; R_n is the n -th section of effective radius of water gushing, m; T is the duration of the water gushing, d.

Additionally, the replenishment of groundwater in the tunnel site area by rainfall should not be overlooked. Water on the surface will infiltrate into the bedrock along weathered rock layers and fault fracture zones [34,35]. With regard to the infiltration of rainfall, the effect of rainfall on water gushing can be represented by the following equations:

$$W_{n(2)} = 0.00274\alpha hS, \quad (12)$$

$$S = 2L_n R_n, \quad (13)$$

where α is the coefficient of infiltration; h is the average annual rainfall, m; S is the catchment area, m^2 .

In the previous method of rainfall infiltration, a fixed catchment area is used to calculate the amount of water gushing in the tunnel, which was expressed as the effective radius of water gushing and the length of the tunnel construction. With a fixed total tunnel length, the accuracy of R_n will directly affect the accuracy of Q . However, complex changes will arise in the groundwater seepage field during the long-term construction process. As a result, R_n is constantly changing. The parameter μ is a characteristic parameter of the rock mass and L_n is a characteristic parameter of the tunnel. Both of them are relatively stable. The two parameters H_n and T are, therefore, used to reflect the evolution of R_n , as follows:

$$R_n = R(T, H_n). \quad (14)$$

For the purpose of this study, the principles of the water equilibrium method are followed. The study area is assumed to be as follows:

1. There is no change in the specific yield of rock above the tunnel, and groundwater is continuously replenished into the rock along the fracture structure;
2. There is no change in the hydraulic connection between the rock aquifers in the tunnel site area for a certain period of time. It is only related to the inherent geological structure, but the tectonic fissures can still change in the case of prolonged groundwater flow;
3. There is no abrupt change in the groundwater head in the tunnel site area within a certain period of time, and it is in a basically stable state;
4. The tunnel is not directly affected by the water system and bedrock fissure water below the elevation where the tunnel is located;
5. Due to the presence of tectonic fissures, the hydraulic connection between neighbouring rock masses is kept stable and, at the same time, they interact with each other. The R_n between adjacent rock sections is slowly changing in a gradient.

4. Case Study

4.1. Background

The highway tunnel under construction studied in this paper is located in Guangdong Province in southern China. It is over 6300 m long and has a maximum depth of 740 m. The tunnel site area is located in a tectonic uplift erosion and denudation low mountain landscape. The stratigraphic lithology of the tunnel site area is mainly Jurassic felsic tuff, Jurassic andesite, and Yanshanian granite. The stratigraphy ranges from new to old, as follows: the Quaternary Pleistocene alluvium (Q_4^{al+pl}), the Quaternary deluvial soils and eluvial soils (Q^{dl+el}), and the Upper Jurassic Gaojiiping group (J_{2+3}^{gj}), etc. The site area

is influenced by the Lotus Mountain deep rift zone. The tunnel crossed a zone of fracture tectonic development with secondary fractures and joints. The rock in the tunnel site area is fractured, which is shown in Figure 2 [36].

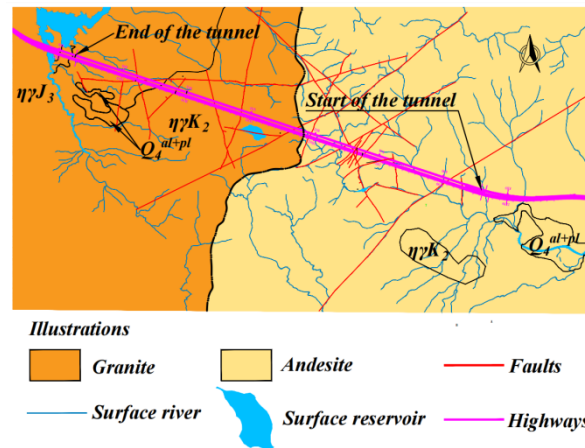


Figure 2. Distribution of fracture structures in the tunnel site area (1:10,000).

The local water resources are abundant, with an average annual rainfall of 1865.6 mm. The results of the hydrogeological survey show that the groundwater in the tunnel site area is mainly supplemented by rainfall. The groundwater types are divided into loose rock pore water and bedrock fracture water. During the construction, a large amount of high-pressure water gushing poured into the tunnel and threatened construction safety, as shown in Figure 3.



Figure 3. Water gushing at the tunnel face. (a) Tunnel face; (b) the vicinity of tunnel face.

4.2. Fuzzy Clustering Method for Identification of the Source of Water Gushing

Due to the high pressure and high flow of water gushing in the excavation phase of the tunnel, the source of water gushing in the tunnel needs to be understood urgently. It is important that the source of water gushing is accurately identified for predicting the amount of water gushing. Data from water samples can be analysed and processed efficiently by fuzzy clustering methods. Samples with a high degree of similarity between them will be classified into one category. These samples from around and inside the tunnel will be differentiated as to whether they originate from the same source. The igneous rocks are relatively rich in minerals. The physicochemical properties of the samples can be derived from tests. The relationship between the samples inside and around the tunnel can be determined with the use of fuzzy clustering analysis [37]. During construction, 14 water samples were taken for testing indoors and analysis, including 10 samples of water gushing in the tunnel for the first time, as well as 4 samples of surface water in the tunnel site area for the second time. The specific implementation steps of this study are as follows:

Step 1. Ten samples of water gushing were analysed by the hydro-geochemistry method. Testing indicators included redox potential, pH, TDS content, conductivity, and water temperature (sample water temperature was measured during field sampling). There were also quantitative elemental characteristics, such as Cl^- , SO_4^{2-} , HCO_3^- , Ca^{2+} , K^+ , Mg^{2+} , and Na^+ . Some test results for the 10 samples from the tunnel are shown in Table 1.

Table 1. Water quality characteristics of ten water gushing samples.

Sample	Sampling Locations	Redox Potential (mV)	pH	TDS (mg/L)	Conductivity ($\mu\text{s}/\text{cm}$)	Temperature ($^\circ\text{C}$)
S1	Walls at K91 + 210	−62.2	8.51	112	174.7	23.5
S2	Walls at K91 + 273	−16	6.85	127	199.1	23.9
S3	Walls at K91 + 300	−15	6.75	128	199.8	24
S4	Walls at K91 + 310	−47.6	7.9	129	201	23.7
S5	Walls at K91 + 314	−35	7.49	127	197.9	23.9
S6	Top of tunnel at ZK94 + 299	−43	7.73	117	182.8	23
S7	Top of tunnel at ZK94 + 250	−98	8.68	120	188.8	23.7
S8	Top of tunnel at ZK94 + 245	−130	9.15	99	154.9	23.8
S9	Walls at ZK94 + 188	−153.3	9.63	122	189.6	23.7
S10	Walls at ZK94 + 198	−105	8.7	123	192.2	24.9

Step 2. The test results were classified using the fuzzy clustering method. The data in Table 1 was initially processed by Equations (1) and (5) to obtain Z_1'' , as expressed in the following Equation (15):

$$Z_1'' = \begin{bmatrix} 0.659 & 0.611 & 0.433 & 0.430 & 0.263 \\ 0.993 & 0.035 & 0.933 & 0.959 & 0.474 \\ 1.000 & 0.000 & 0.967 & 0.974 & 0.526 \\ 0.764 & 0.399 & 1.000 & 1.000 & 0.368 \\ 0.855 & 0.257 & 0.933 & 0.933 & 0.474 \\ 0.798 & 0.340 & 0.600 & 0.605 & 0.000 \\ 0.400 & 0.670 & 0.700 & 0.735 & 0.368 \\ 0.168 & 0.833 & 0.000 & 0.000 & 0.421 \\ 0.000 & 1.000 & 0.767 & 0.753 & 0.368 \\ 0.349 & 0.677 & 0.800 & 0.809 & 1.000 \end{bmatrix}. \tag{15}$$

Step 3. According to Equation (7) to Equation (8), Z_1'' was processed for the first time to give the original matrix C_1 , which was shown in the following Equation (16):

$$C_1 = \begin{bmatrix} 1.0000 & 0.5880 & 0.5641 & 0.6551 & 0.6556 & 0.8083 & 0.7974 & 0.6616 & 0.6322 & 0.6081 \\ 0.5880 & 1.0000 & 0.9701 & 0.8164 & 0.8928 & 0.6859 & 0.6190 & 0.2800 & 0.4228 & 0.5634 \\ 0.5641 & 0.9701 & 1.0000 & 0.7993 & 0.9100 & 0.7252 & 0.7324 & 0.5692 & 0.5503 & 0.6761 \\ 0.6551 & 0.8164 & 0.7993 & 1.0000 & 0.9100 & 0.7243 & 0.7530 & 0.3486 & 0.5796 & 0.6524 \\ 0.6556 & 0.8928 & 0.9100 & 0.9100 & 1.0000 & 0.7252 & 0.7164 & 0.3483 & 0.5248 & 0.6482 \\ 0.8083 & 0.6859 & 0.7252 & 0.7243 & 0.7252 & 1.0000 & 0.7324 & 0.4930 & 0.5424 & 0.5176 \\ 0.7974 & 0.6190 & 0.7324 & 0.7530 & 0.7164 & 0.7324 & 1.0000 & 0.5692 & 0.7865 & 0.7364 \\ 0.6616 & 0.2800 & 0.5692 & 0.3486 & 0.3483 & 0.4930 & 0.5692 & 1.0000 & 0.5503 & 0.4698 \\ 0.6322 & 0.4228 & 0.5503 & 0.5796 & 0.5248 & 0.5424 & 0.7865 & 0.5503 & 1.0000 & 0.6761 \\ 0.6081 & 0.5634 & 0.6761 & 0.6524 & 0.6482 & 0.5176 & 0.7364 & 0.4698 & 0.6761 & 1.0000 \end{bmatrix}. \tag{16}$$

The transitive closure $t(C_1) = C_1^4 = C_1^8$ could be found for the 4-th time. Then, $t(C_1)$ was given in Equation (17), as follows:

$$t(C_1) = C_1^4 = C_1^8 = \begin{bmatrix} 1.0000 & 0.7530 & 0.7530 & 0.7530 & 0.7530 & 0.8083 & 0.7974 & 0.6616 & 0.7865 & 0.7364 \\ 0.7530 & 1.0000 & 0.9701 & 0.9100 & 0.9100 & 0.7530 & 0.7530 & 0.6616 & 0.7530 & 0.7364 \\ 0.7530 & 0.9701 & 1.0000 & 0.9100 & 0.9100 & 0.7530 & 0.7530 & 0.6616 & 0.7530 & 0.7364 \\ 0.7530 & 0.9100 & 0.9100 & 1.0000 & 0.9100 & 0.7530 & 0.7530 & 0.6616 & 0.7530 & 0.7364 \\ 0.7530 & 0.9100 & 0.9100 & 0.9100 & 1.0000 & 0.7530 & 0.7530 & 0.6616 & 0.7530 & 0.7364 \\ 0.8083 & 0.7530 & 0.7530 & 0.7530 & 0.7530 & 1.0000 & 0.7974 & 0.6616 & 0.7865 & 0.7364 \\ 0.7974 & 0.7530 & 0.7530 & 0.7530 & 0.7530 & 0.7974 & 1.0000 & 0.6616 & 0.7865 & 0.7364 \\ 0.6616 & 0.6616 & 0.6616 & 0.6616 & 0.6616 & 0.6616 & 0.6616 & 1.0000 & 0.6616 & 0.6616 \\ 0.7865 & 0.7530 & 0.7530 & 0.7530 & 0.7530 & 0.7865 & 0.7865 & 0.6616 & 1.0000 & 0.7364 \\ 0.7364 & 0.7364 & 0.7364 & 0.7364 & 0.7364 & 0.7364 & 0.7364 & 0.6616 & 0.7364 & 1.0000 \end{bmatrix} \quad (17)$$

Yang et al. [38] set $\lambda = 0.6173$ for the classification of hydraulic fissures. Referring to Section 2 for the definition of λ , it was more reasonable to set the optimal classification threshold of $\lambda = 0.6616$ in this paper. The classification results were shown in Figure 4.

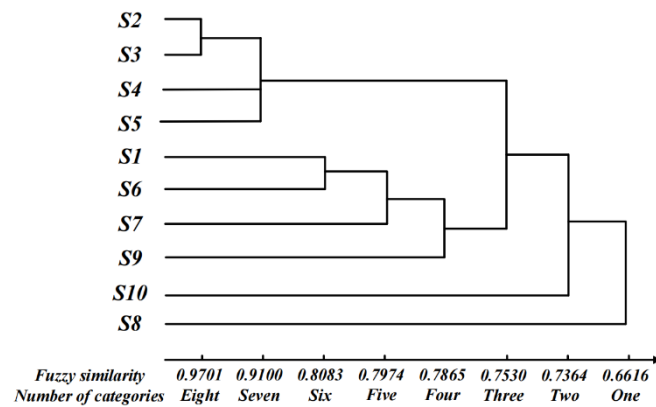


Figure 4. Fuzzy clustering analysis results for 10 water gushing samples in the tunnel.

From Figure 4, the following can be seen: $\lambda_{min} > 0.6$, the ten samples in the tunnel were relevant, according to Section 2. When $\lambda = 0.6616$, the 10 water samples from the gushing in the tunnel could be classified into the same category. This result indicated that the 10 water samples in the tunnel were similar and that they originated from the same source.

For comparison with four samples from around the tunnel, samples S1 and S10 were selected to further analyse whether the water gushing in the tunnel originated from the surface water system. For the second time, four samples of surface water in the tunnel site area were taken for analysis and compared with samples S1 and S10. Repeating the above three steps, the samples were characterised for their elemental content of Cl^- , SO_4^{2-} , HCO_3^- , Ca^{2+} , K^+ , Mg^{2+} , and Na^+ . The test results are shown in Appendix A. Similarly, Z_2'' was obtained by preliminary processing of the data in Appendix A through Equation (1) to Equation (5). It was represented as follows:

$$Z_2'' = \begin{bmatrix} 0.898 & 0.905 & 0.908 & 0.269 & 1.000 & 1.000 & 1.000 & 1.000 & 0.919 & 0.536 \\ 1.000 & 1.000 & 1.000 & 0.077 & 0.505 & 1.000 & 0.917 & 0.178 & 1.000 & 1.000 \\ 0.583 & 0.054 & 0.042 & 0.000 & 0.001 & 0.035 & 0.008 & 0.000 & 0.000 & 0.243 \\ 0.417 & 0.239 & 0.185 & 0.385 & 0.271 & 0.255 & 0.223 & 0.368 & 0.475 & 0.160 \\ 0.000 & 0.000 & 0.000 & 1.000 & 0.030 & 0.000 & 0.000 & 0.196 & 0.071 & 0.000 \\ 0.032 & 0.016 & 0.013 & 0.462 & 0.000 & 0.005 & 0.001 & 0.258 & 0.061 & 0.062 \end{bmatrix} \quad (18)$$

Furthermore, the raw matrix C_2 was represented as follows:

$$C_2 = \begin{bmatrix} 1.0000 & 0.6515 & 0.1944 & 0.3967 & 0.1295 & 0.1707 \\ 0.6515 & 1.0000 & 0.2510 & 0.3846 & 0.1178 & 0.1706 \\ 0.1944 & 0.2510 & 1.0000 & 0.7234 & 0.6194 & 0.7506 \\ 0.3967 & 0.3846 & 0.7234 & 1.0000 & 0.6783 & 0.7527 \\ 0.1295 & 0.1178 & 0.6194 & 0.6783 & 1.0000 & 0.8268 \\ 0.1707 & 0.1706 & 0.7506 & 0.7527 & 0.8268 & 1.0000 \end{bmatrix}. \tag{19}$$

The transitive closure $t(C_2) = C_2^4 = C_2^8$ was found for the 4-th time, which was shown as follows:

$$t(C_2) = C_2^4 = C_2^8 = \begin{bmatrix} 1.0000 & 0.6515 & 0.3967 & 0.3967 & 0.3967 & 0.3967 \\ 0.6515 & 1.0000 & 0.3967 & 0.3967 & 0.3967 & 0.3967 \\ 0.3967 & 0.3967 & 1.0000 & 0.7506 & 0.7506 & 0.7506 \\ 0.3967 & 0.3967 & 0.7506 & 1.0000 & 0.7527 & 0.7527 \\ 0.3967 & 0.3967 & 0.7506 & 0.7527 & 1.0000 & 0.8268 \\ 0.3967 & 0.3967 & 0.7506 & 0.7527 & 0.8268 & 1.0000 \end{bmatrix} \tag{20}$$

The optimal classification threshold λ was set at 0.6515 and the classification results were shown in Figure 5.

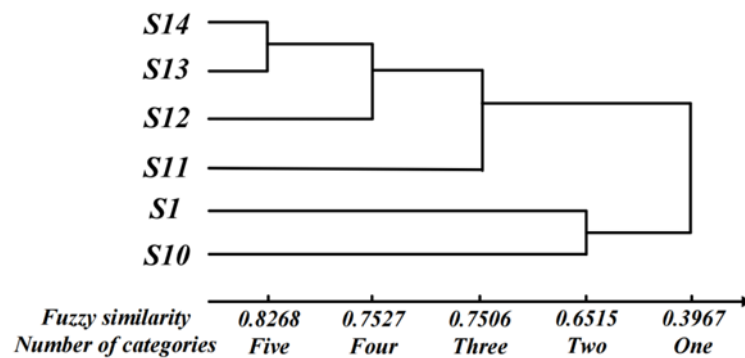


Figure 5. Fuzzy clustering analysis results for water gushing samples in the tunnel.

From Figure 5, it could be seen that $0.3 < \lambda_{min} < 0.6$, so there was a weak correlation between the samples inside (S1 and S10) and outside (S11~S14) the tunnel, according to Section 2. As already mentioned in the previous section, samples S1 and S10 had been classified as one. When $\lambda = 0.6515$, the samples could be classified into two categories. The new samples S11, S12, S13, and S14 were grouped together as a new category, and the S1 and S10 were grouped in the other category. According to the fuzzy clustering method, the results of analysis showed that there was a certain difference in the physicochemical composition between the samples from the tunnel and the water system outside. In the early stages of tunnel construction excavation, the water gushing into the tunnel was mainly derived from water in the bedrock fracture, partly from surface infiltration of precipitation.

4.3. Prediction of Water Gushing Based on the Effective Radius of the Dynamic

According to Section 3, water gushing in the tunnel under construction is mainly from the water inside the bedrock fracture. Due to the time span of the construction process, the infiltration of rainfall will have a non-negligible effect on groundwater replenishment. Therefore, in this section the monitoring data for the amount of water gushing will be substituted into Equation (9) to Equation (14) for regression analysis. The expression for R_n is obtained, and then the tunnel gushing calculation equation can be derived.

4.3.1. Defining Parameters

The tunnel was divided into several calculation sections based on the characteristics of the water-bearing medium, the nature of the surrounding rock, the grade of the surrounding rock, the crossing of the fracture zone, the width and inclination of the fracture zone, as well as the construction schedule of the different surrounding rocks in the tunnel. The excavated and rock-disturbed part of the right tunnel were divided along the line into N sections, each with a length L_n of 10 m to 110 m. As the tunnel was excavated, N would continue to increase. Eventually the total length of the N segments would be equal to the actual length of the tunnel excavation. The amount of water gushing was recorded daily at the inlet of the right tunnel. The time was calculated from the first water gushing in the tunnel. The five study nodes were set as follows: ① $T = 150$ d, $N = 23$; ② $T = 200$ d, $N = 24$; ③ $T = 250$ d, $N = 25$; ④ $T = 300$ d, $N = 26$; ⑤ $T = 350$ d, $N = 27$.

According to the data from the engineering geological survey, the specific selection parameters for each section were shown in Figure 6. The selection of parameters for each segment was described as follows.

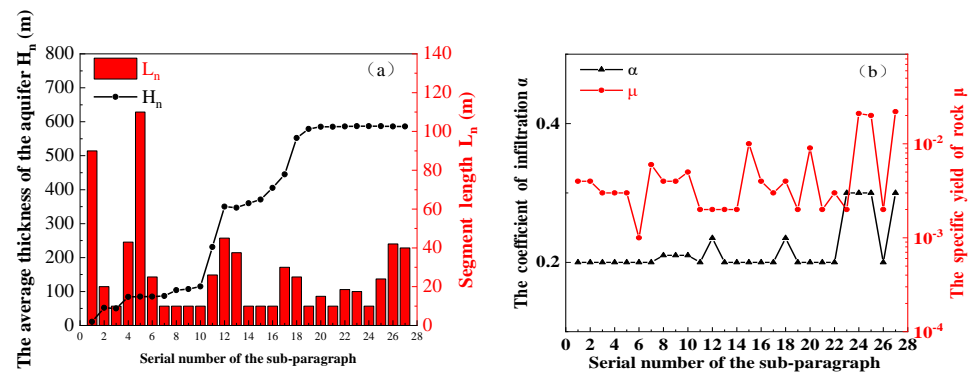


Figure 6. Distribution of parameters by segments. (a) L_n and H_n ; (b) μ and α .

The average thickness of the aquifers in each segment ranged from 11 m to 587 m. The specific yields of rock in each study section were from 0.001 to 0.025. The rainfall infiltration coefficients for weathered rock layers on the mountain surface were from 0.2 to 0.3. The average annual rainfall in the tunnel site area was 1865.6 mm.

4.3.2. Effective Radius of the Dynamic

Substituting the recorded data into Equation (9) to Equation (13), the variation pattern of the R_n corresponding to each segment was obtained, as shown in Figure 7.

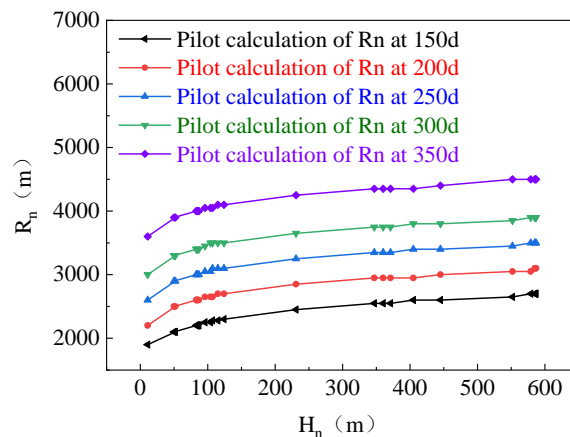


Figure 7. Variation pattern of radius of influence R_n for each segment.

As can be seen from Figure 7, R_n increased as T and H_n increased. The rate of increase of R_n was decreasing with an overall non-linear increase. In order to reflect the mathematical relationship better between the above three factors, a power function model was chosen for the regression analysis of R_n and H_n , with the condition of a defined duration of water gushing T . Here, R_n could be set as follows:

$$R_n = a(H_n)^b \tag{21}$$

The regression results of Equation (21) were shown in Figure 8. In order to present the relationship better between R_n , T , and H_n through mathematical expressions, power function representations and quadratic equations were used to represent the parameters a and b . At this point, they could be set as follows:

$$R_n = R(T, H_n) = a_1 T^{b_1} H_n^{a_2 T^2 + b_2 T + c_2} \tag{22}$$

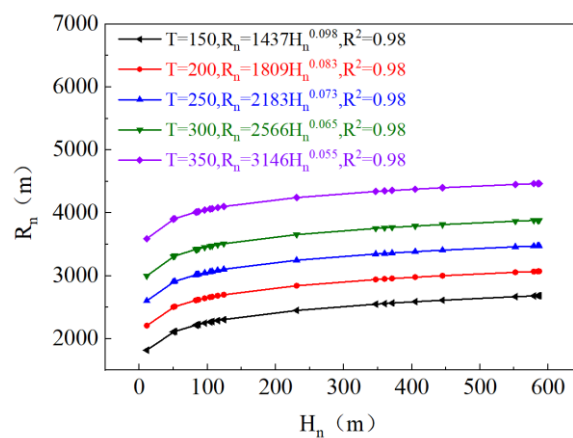


Figure 8. R_n regression results.

Based on the data in Figure 8, Equation (23) was derived by regression, as follows:

$$\begin{cases} a_1 = 12.16 \\ b_1 = 0.94 \end{cases}, R^2 = 0.99 \tag{23}$$

$$\begin{cases} a_2 = 4.63 \times 10^{-7} \\ b_2 = -4.32 \times 10^{-4} \\ c_2 = 0.15 \end{cases}, R^2 = 0.99.$$

Additionally, Equation (22) could be set as follows:

$$R_n = R(T, H_n) = 12.16 T^{0.9} H_n^{4.63 \times 10^{-7} T^2 - 4.32 \times 10^{-4} T + 0.15}, (T \leq 350). \tag{24}$$

The relationship between R_n , T , and H_n was reflected by Equation (24). As the storage of water from bedrock fractures was limited, R_n did not increase indefinitely. Additionally, Equation (24) was used to calculate R_n only for one rainfall cycle after the occurrence of the water gushing. Equation (24) was substituted into Equation (9) to (13) and simplified to obtain Equation (25), as follows:

$$Q = \sum_{n=1}^N (W_{n(1)} + W_{n(2)}) = \sum_{n=1}^N (12.16 \mu H_n T^{-0.1} + 0.06576 \alpha h T^{0.9}) L_n \times H_n^{4.63 \times 10^{-7} T^2 - 4.32 \times 10^{-4} T + 0.15}. \tag{25}$$

The results of calculation, derived from Equation (25), were shown in Figure 9 as a comparison with dynamic monitoring data.

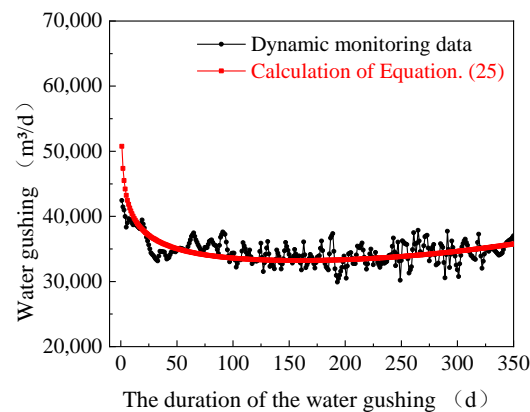


Figure 9. Comparison of calculated results with dynamic monitoring records.

From Figure 9, it can be seen that the front end of the curve had a plummeting trend, with a relatively flat middle and a slight rise at the end. According to the amount of water gushing, the period of water gushing could be divided into three stages. The first stage was a time period of 1 to 6 days, and the stage had a negative growth rate of greater than 10% for a single day. The second stage was 7 to 170 days into a period of larger water gushing, with a negative growth rate of less than 10% in single day of water gushing. The third stage was 170 days after. This stage of water gushing increased very slowly, with a positive single day growth rate of greater than 0.01%.

4.4. Discussion

The results based on the source of the water showed that the water gushing was released primarily from bedrock fractures, but was still weakly influenced by the surface water system. From Figure 9, it was seen that the curve was abrupt and starts with a large value in the first stage. This was the stage where the bedrock fracture water continued to gush into the tunnel in large quantities in a short period of time. The site conditions were consistent with those expressed at this stage.

The second stage curve was smooth. It showed that the bedrock fracture water above the tunnel site area was reduced at this time. Bedrock fracture water and infiltrated rainfall from the adjacent areas of the tunnel site were continuously replenished into the rock above the tunnel site along the fracture structure. The site conditions were also consistent with those expressed at this stage.

In the third stage, the curve was slowly increasing, which reflected the fact that the water gushing in the tunnel at this stage were influenced by factors, such as rainfall and changes in tectonic fissures. Comparing the left and right halves of Equation (23), the following was obtained:

$$\frac{W_{n(1)}}{W_{n(2)}} = \frac{12.16\mu H_n}{0.06576\alpha h T}. \quad (26)$$

Although it was assumed in this paper that the variation in H was negligible to represent the strong water transport capacity of the bedrock, H should in practice be decreasing as T increases. Hence, Equation (24) should be constantly converging to zero with the rest of parameters remaining constant.

Overall, the impact of water from the bedrock fracture on the water gushing would become smaller with the increase in the duration of the water gushing, and the impact of the infiltration of water from the surface would become greater. The error between the calculated results and the actual monitoring values was within 10%, except for the 1–6 days, when the error in the calculated results ranged from 10% to 20%. In the study of the erosion and seepage process of the surrounding rock and the characteristics of the water intake of the fault fracture zone, other scholars also adopted a three- or four-stage model to use in

the study [39,40]. Therefore, it was reasonable to divide the period of water gushing into three stages in this study.

Meanwhile, the method of rainfall infiltration and method of the runoff module number of the groundwater were applied for comparison with the methodology of this article. As their approach to prediction differed from the method in this study, some of the results with an average duration of 150 d, 200 d, 250 d, 300 d, and 350 d for predicted water gushing from the hydrogeological investigation phase of this project were selected for comparison, which were shown in Table 2.

Table 2. Comparative analysis of water gushing.

Methods	The Average Duration of Water Gushing (d)				
	150	200	250	300	350
Method of rainfall infiltration	7701	10,268	12,836	15,403	17,456
Method of the runoff module number of the groundwater	5854	7805	9757	11,708	13,269
Methodology of this article	36,510	36,020	35,274	34,800	34,085
Dynamic monitoring data	38,198	36,174	35,231	34,736	33,578

From Table 2, it could be seen that the results from the methodology of this article were closer to the dynamic monitoring data, while the other methods had very different results. It was worth noting that method of rainfall infiltration and method of the runoff module number of the groundwater were not sufficiently concerned with the static water from the bedrock fracture in the prediction of water gushing, and they focused more on rainfall and surface water recharge to groundwater. That was the main cause of the error. On the other hand, the catchment area was not expressed by a fixed value when predicting water gushing. It was related to the changes in the average thickness of the aquifer and the duration of the water gushing. This was another cause of error. In contrast, the approach in this paper was more concerned with the water from the bedrock fracture. The fuzzy clustering method was used to monitor the release of water from the bedrock fracture and the infiltration of rainfall for replenishment. The dynamic effective radius of water gushing was applied to reflect the changes in catchment area, which was why it had fewer errors.

4.5. Subsequent On-Site Validation

As a further test of the accuracy of Equation (25), the subsequent construction section K91 + 700 to K91 + 950 of the tunnel was selected. The total length of this tunnel section was 250 m, with a total of 42 days of construction excavation. It was influenced by the tensor fault F2-6, which was given in Figure 10.

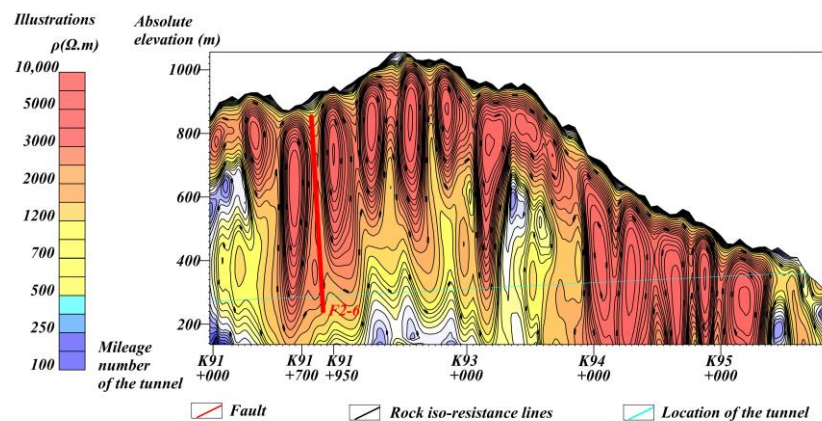


Figure 10. The relationship between the fault F2-5 and the tunnel section.

The average thickness of the aquifer H_n in the water-rich fault fracture zone was approximately 587 m. The surface of the mountain was a weathered layer of andesite with

a precipitation infiltration coefficient of 0.25 to 0.3. The 250 m long section was divided into six successive sections from A to F with a difference gradient of 0.0005 based on the difference in rock feed. During construction, the timing of water gushing was recorded for each section. The effects of the amount of water seepage from adjacent tunnel sections were ignored. The specific parameters were detailed in Figure 11.

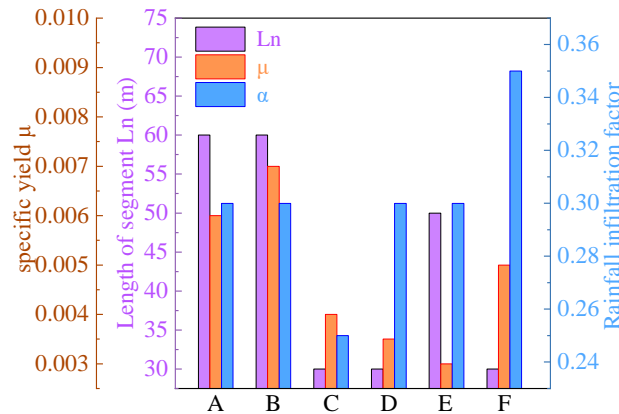


Figure 11. Parameters of each segment.

The parameters in Figure 11 were substituted into Equation (24) for the calculation. The value of the variation of R_n with T for this construction section was obtained. The calculations of R_n at each time point were substituted into Equation (25), and the calculated value of water gushing from the section K91 + 700 to K91 + 950 was obtained. The calculated results were compared with the dynamic monitoring values, which were shown in Figure 12.

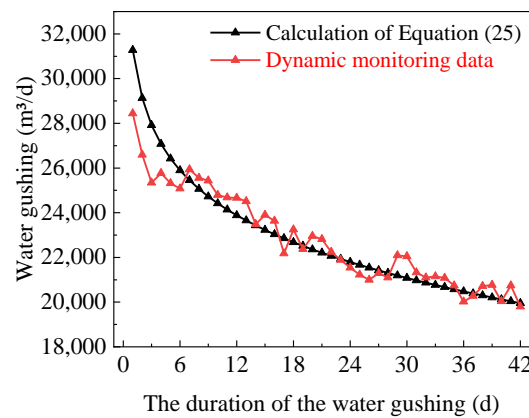


Figure 12. Results of comparison of calculated values with dynamic monitoring data from K91 + 700 to K91 + 950.

As can be seen in Figure 12, the trend between the calculated value curve and the dynamic monitoring data curve was generally consistent. Both of them decreased when the time increased. The calculated value of water gushing within one to six days was slightly greater than the actual monitored value, with an average error of 7%. Some fluctuations in the results of dynamic monitoring occurred between days 7 and 42. Overall the calculated values were relatively close to the recorded values. The maximum error was less than 5%.

5. Conclusions

1. The introduction of fuzzy clustering method ensured that the water gushing source in the igneous rock area could be effectively identified. The similarity index of $\lambda_{min} = 0.3967$ indicated that the water gushing out of the tunnel had a low correlation

- with the surface water. They came mainly from within the rock mass. The collection of water samples should accompany the whole process of tunnel excavation. This is important for the dynamic prediction of tunnel excavation water gushing.
2. A new and more accurate method has been proposed and restructured to dynamically predict the water gushing in deep underground, extra-long tunnels in igneous areas. The overall error in prediction results was less than 10%, which was more accurate compared to the method of rainfall infiltration and the method of the runoff module number of the groundwater. Moreover, the supplementation of bedrock fracture water by precipitation should not be neglected.
 3. By means of the results of the dynamic data, the effective radius of water gushing during a rainfall cycle was positively correlated with the average thickness of the aquifer in the rock formation. When a tunnel was built in a fracture zone, it should be considered to cross a mountain with a small average thickness of aquifer or to reduce the depth of burial as much as possible. As a result, the risk of water gushing was reduced.
 4. The period of water gushing was divided into three stages in this study. According to the improved method for prediction of water gushing, the impact of the water from the bedrock fracture on the water gushing would become smaller with the increase in the duration of the water gushing, and the impact of the infiltration of water from the surface would become greater.

Author Contributions: W.Z. contribution was is data collection and collation, and proposed the research ideas and methodology for the first draft. X.Z. and B.W. completed the first draft under the guidance of W.Z. and W.W. W.W. suggested changes to the thesis and was responsible for all expenses. X.C. was responsible for the monitoring and recording of field data. All authors have read and agreed to the published version of the manuscript.

Funding: This work was supported by Project of Guangdong Water Resources Department: Experimental and Applied Research on the Durability of Concrete under Marine Erosion Environment (2015K23), Water Resources Science and Technology Tackling Project of Guangdong Province: Study on the Suitability of RSM Geotechnical Consolidation Agent for Seawall Reinforcement Project (2015-16), the Regulations Preparation Project of the Ministry of Transport of the People’s Republic of China, “Regulations for Hydrogeological Investigation of Highway Cross-Ridge Tunnels” (CECS G-2019-1-008), Science and Technology Innovation Project ((2021) R&D YF-014, YF-015) of Guangdong Communication Planning & Design Institute Group Co., Ltd., Supported by Guangdong Provincial Student Innovation Project (S202110564060).

Institutional Review Board Statement: Not applicable.

Informed Consent Statement: Not applicable.

Data Availability Statement: Not applicable.

Conflicts of Interest: The authors declare no conflict of interest.

Appendix A. Characteristics of the Macronutrient Ion Content of the Six Water Samples

Samples	Sampling Locations	PH	Conductivity ($\mu\text{s}/\text{cm}$)	TDS (mg/L)	Cl^- (mg/L)	SO_4^{2-} (mg/L)	HCO_3^- (mg/L)
S1	Walls at K91 + 210	8.51	174.7	112	4.74	10.59	128.14
S10	Walls at ZK94 + 198	8.7	192.2	123	4.69	7.27	128.14
S11	River 2.1 km left of tunnel ZK92 + 800	7.92	18	9	4.67	3.89	22.51
S12	River 300 m left of tunnel K90 + 220	7.61	52	26	4.77	5.7	46.61
S13	The reservoir above the tunnel	6.83	8	4	4.93	4.08	18.72
S14	River at tunnel K92 + 500	6.89	11	5.5	4.79	3.88	19.31

References

1. Li, X.; Zhang, P.; He, Z.; Huang, Z.; Cheng, M.; Guo, L. Identification of geological structure which induced heavy water and mud inrush in tunnel excavation: A case study on Lingjiao tunnel. *Tunn. Undergr. Sp. Tech.* **2017**, *69*, 203–208. [\[CrossRef\]](#)
2. Nikvar Hassani, A.; Katibeh, H.; Farhadian, H. Numerical analysis of steady-state groundwater inflow into Tabriz line 2 metro tunnel, northwestern Iran, with special consideration of model dimensions. *B Eng. Geol. Environ.* **2016**, *75*, 1617–1627. [\[CrossRef\]](#)
3. Liu, J.; Chen, W.; Yuan, J.; Li, C.; Zhang, Q.; Li, X. Groundwater control and curtain grouting for tunnel construction in completely weathered granite. *B Eng. Geol. Environ.* **2018**, *77*, 515–531. [\[CrossRef\]](#)
4. Shi, S.; Xie, X.; Wen, Z.; Zhou, Z.; Li, L.; Song, S.; Wu, Z. Intelligent Evaluation System of Water Inrush in Roadway (Tunnel) and Its Application. *Water* **2018**, *10*, 997. [\[CrossRef\]](#)
5. Golian, M.; Katibeh, H.; Singh, V.P.; Ostad-Ali-Askari, K.; Rostami, H.T. Prediction of tunnelling impact on flow rates of adjacent extraction water wells. *Q. J. Eng. Geol. Hydrogeol.* **2019**, *53*, 236–251. [\[CrossRef\]](#)
6. Li, X.; Li, Y.; Chang, C.; Tan, B.; Chen, Z.; Sege, J.; Wang, C.; Rubin, Y. Stochastic, goal-oriented rapid impact modeling of uncertainty and environmental impacts in poorly-sampled sites using ex-situ priors. *Adv. Water Resour.* **2018**, *111*, 174–191. [\[CrossRef\]](#)
7. Gokdemir, C.; Li, Y.; Rubin, Y.; Li, X. Stochastic modeling of groundwater drawdown response induced by tunnel drainage. *Eng. Geol.* **2022**, *297*, 106529. [\[CrossRef\]](#)
8. El Tani, M. Helmholtz evolution of a semi-infinite aquifer drained by a circular tunnel. *Tunn. Undergr. Sp. Tech.* **2010**, *25*, 54–62. [\[CrossRef\]](#)
9. Niu, F.; Cai, Y.; Liao, H.; Li, J.; Tang, K.; Wang, Q.; Wang, Z.; Liu, D.; Liu, T.; Liu, C.; et al. Unfavorable Geology and Mitigation Measures for Water Inrush Hazard during Subsea Tunnel Construction: A Global Review. *Water* **2022**, *14*, 1592. [\[CrossRef\]](#)
10. Liu, J.; Li, Z.; Zhang, X.; Weng, X. Analysis of Water and Mud Inrush in Tunnel Fault Fracture Zone—A Case Study of Yonglian Tunnel. *Sustainability* **2021**, *13*, 9585. [\[CrossRef\]](#)
11. Zhang, Z.; Xu, P.; Zhang, H.; Zhang, K. Dynamic Change Characteristics of Groundwater Affected by Super-Long Tunnel Construction in the Western Mountainous Area of China. *Sustainability* **2019**, *11*, 2329. [\[CrossRef\]](#)
12. Sun, W.; Xue, Y.; Li, T.; Liu, W. Multi-field Coupling of Water Inrush Channel Formation in a Deep Mine with a Buried Fault. *Mine Water Environ.* **2019**, *38*, 528–535. [\[CrossRef\]](#)
13. Li, G.; Ma, W.; Tian, S.; Hongbo, Z.; Huabin, F.; Zou, W. Groundwater Inrush Control and Parameters Optimization of Curtain Grouting Reinforcement for the Jingzhai Tunnel. *Geofluids* **2021**, *2021*, 6634513. [\[CrossRef\]](#)
14. Wu, J.; Wang, X.; Wu, L.; Lu, Y.; Han, Y. Parametric Study of Water Inrush in a Tunnel Crossing a Fault Based on the “Three Zones” Fault Structure. *KSCE J. Civ. Eng.* **2022**, *26*, 3600–3619. [\[CrossRef\]](#)
15. Gu, H.; Ma, F.; Guo, J.; Li, K.; Lu, R. Hydrochemistry, multidimensional statistics, and rock mechanics investigations for Sanshandao Gold Mine, China. *Arab. J. Geosci.* **2017**, *10*, 62. [\[CrossRef\]](#)
16. Yin, H.; Zhao, H.; Xie, D.; Sang, S.; Shi, Y.; Tian, M. Mechanism of mine water inrush from overlying porous aquifer in Quaternary: A case study in Xinhe Coal Mine of Shandong Province, China. *Arab. J. Geosci.* **2019**, *12*, 163. [\[CrossRef\]](#)
17. Saberinasr, A.; Morsali, M.; Hashemnejad, A.; Hassanpour, J. Determining the origin of groundwater elements using hydrochemical data (case study: Kerman water conveyance tunnel). *Environ. Earth Sci.* **2019**, *78*, 198. [\[CrossRef\]](#)
18. Wang, Y.; Zhou, M.-r.; Yan, P.-c.; He, C.-y.; Liu, D. Identification of Coalmine Water Inrush Source with PCA-BP Model Based on Laser-Induced Fluorescence Technology. *Spectrosc. Spect. Anal.* **2017**, *37*, 978–983.
19. Chen, Y.; Zhu, S.; Xiao, S. Discussion on controlling factors of hydrogeochemistry and hydraulic connections of groundwater in different mining districts. *Nat. Hazards* **2019**, *99*, 689–704. [\[CrossRef\]](#)
20. Kang, X.; Luo, S.; Xu, M.; Zhang, Q.; Yang, Y. Dynamic estimating the karst tunnel water inflow based on monitoring data during excavation. *Acta Carsologica.* **2019**, *48*, 117–127. [\[CrossRef\]](#)
21. He, W.; Hayatdavoudi, A.; Shi, H.; Sawant, K.; Huang, P. A Preliminary Fractal Interpretation of Effects of Grain Size and Grain Shape on Rock Strength. *Rock Mech. Rock Eng.* **2019**, *52*, 1745–1765. [\[CrossRef\]](#)
22. Aligholi, S.; Lashkaripour, G.R.; Ghafoori, M.; Azali, S.T. Evaluating the Relationships Between NTNU/SINTEF Drillability Indices with Index Properties and Petrographic Data of Hard Igneous Rocks. *Rock Mech. Rock Eng.* **2017**, *50*, 2929–2953. [\[CrossRef\]](#)
23. Huang, C.; Zhang, S.; Wu, S.; Gao, Y. Research and application of a comprehensive forecasting system for tunnels in water-bearing fault fracture zones: A case study. *Arab. J. Geosci.* **2022**, *15*, 171. [\[CrossRef\]](#)
24. Akara, M.M.; Reeves, D.M.; Parashar, R. Impact of horizontal spatial clustering in two-dimensional fracture networks on solute transport. *J. Hydrol.* **2021**, *603*, 127055. [\[CrossRef\]](#)
25. de Palézieux, L.; Loew, S. Long-term transient groundwater pressure and deep infiltration in Alpine mountain slopes (Poschiavo Valley, Switzerland). *Hydrogeol. J.* **2019**, *27*, 2817–2834. [\[CrossRef\]](#)
26. Chang, Q.; Sun, X.; Zhou, H.; Shi, X. A multivariate matrix model of analysing mine water bursting and its application. *Desalin. Water Treat.* **2018**, *123*, 20–26. [\[CrossRef\]](#)
27. Zhou, F.; Zhang, W.; Sun, K.; Shi, B. Optimized Fuzzy Clustering Method for Health Monitoring of Shield Tunnels. *Trans. Nanjing Univ. Aeronaut. Astronaut.* **2015**, *32*, 325–333.
28. Liu, Y.; Chen, W.; Chen, W.; Chen, Y.; Ma, L.; Meng, Z. Reconstruction Method of Ocean Front Model Based on Fuzzy Cluster Analysis of Sound Speed Profile. *IEEE Access* **2021**, *9*, 112714–112725. [\[CrossRef\]](#)

29. Jiao, Y.; Liu, H.; Zhang, P.; Wang, X.; Wei, H. Unsupervised Performance Evaluation Strategy for Bridge Superstructure Based on Fuzzy Clustering and Field Data. *Sci. World J.* **2013**, *2013*, 427072. [[CrossRef](#)]
30. Liu, H.; Jiao, Y.; Cheng, Y.; Gong, Y. Reduction of Uncertainties for Damage Identification of Bridge Based on Fuzzy Nearness and Modal Data. *J. Appl. Math.* **2012**, *2012*, 812932. [[CrossRef](#)]
31. Yang, M.; Wang, C. Clustering Methods Based on Weighted Quasi-Arithmetic Means of T-Transitive Fuzzy Relations. *Int. J. Uncertain. Fuzz.* **2015**, *23*, 715–733. [[CrossRef](#)]
32. Yongsheng, L.; Yunchao, D.; Danni, Z.; Shengzhang, Z.; Ahmadi, F. Karst hydrogeological characteristics and water-gushing prediction of Dejiang Tunnel in Guizhou Province. *Water Resour. Hydropower Eng.* **2020**, *51*, 63–70.
33. Liu Yan, Z.H. Characteristics of inferior variation of water environment and regulating capacity of groundwater reservoir in Jinghui Canal Irrigation District of China. *Trans. CSAE* **2011**, *27*, 19–24.
34. Shi, G.; Gu, G.; Zhou, H.; Tao, Z.; Pan, H.; Tang, T.; Yin, Q. Stability Monitoring and Analysis of High and Steep Slope of a Hydropower Station. *Geofluids* **2020**, *2020*, 8840269. [[CrossRef](#)]
35. Lo Russo, S.; Gnani, L.; Peila, D.; Suozzi, E. Rough evaluation of the water-inflow discharge in abandoned mining tunnels using a simplified water balance model: The case of the Cogne iron mine (Aosta Valley, NW Italy). *Environ. Earth Sci.* **2013**, *70*, 2753–2765. [[CrossRef](#)]
36. Zhang, W.; Zhou, X.; Wei, W.; Cheng, X. Risk Assessment of Water Inrush in Tunnels: A Case Study of a Tunnel in Guangdong Province, China. *Sustainability* **2022**, *14*, 11443. [[CrossRef](#)]
37. Ahmadi, F.; Eilbeigy, M. Evaluation of water source origin around Kerman tunnel, Iran: Water transfer tunnel path using 2H, 3H, 18O, and 34S isotopes. *Arab. J. Geosci.* **2021**, *14*, 993. [[CrossRef](#)]
38. Yang, G.; Chen, C.; Gao, S.-L.; Feng, B. Study on the height of water flowing fractured zone based on analytic hierarchy process and fuzzy clustering analysis method. *J. Min. Saf. Eng.* **2015**, *32*, 206–212.
39. Ma, D.; Duan, H.; Li, X.; Li, Z.; Zhou, Z.; Li, T. Effects of seepage-induced erosion on nonlinear hydraulic properties of broken red sandstones. *Tunn. Undergr. Sp. Tech.* **2019**, *91*, 102993. [[CrossRef](#)]
40. Zhao, X.; Yang, X. Experimental study on water inflow characteristics of tunnel in the fault fracture zone. *Arab. J. Geosci.* **2019**, *12*, 399. [[CrossRef](#)]